AIAA JOURNAL
Vol. 37, No. 8, August 1999

Toward Perfectly Absorbing Boundary Conditions for Euler Equations

M. Ehtesham Hayder*
Rice University, Houston, Texas 77005-1892
Fang Q. Hu†
Old Dominion University, Norfolk, Virginia 23529
and
M. Yousuff Hussaini‡
Florida State University, Tallahassee, Florida 32306-3075

We examine the effectiveness of absorbing layers as nonreflecting computational boundaries for the Euler equations. The absorbing-layer equations are simply obtained by splitting the governing equations in the coordinate directions and introducing absorption coefficients in each split equation. This methodology is similar to that used by Berenger for the numerical solutions of Maxwell's equations. Specifically, we apply this methodology to three physical problems—shock-vortex interactions, a plane free shear flow, and an axisymmetric jet—with emphasis on acoustic wave propagation. Our numerical results indicate that the use of absorbing layers effectively minimizes numerical reflection in all three problems considered.

I. Introduction

THE proper treatment of computational boundaries is crucial for any numerical solution to a set of partial differential equations that governs fluid motion or wave propagation in a medium. Various techniques have been developed to minimize the reflection of outgoing waves. A review can be found in Givoli.[1] Numerical boundary conditions based on the characteristics of the relevant linearized equations and their asymptotic solutions in the far field have been widely used. However, such boundary conditions are not satisfactory if the outflow is nonlinear or involves multidirectional waves. As a possible remedy, a buffer zone abutting the computational boundary, in which the governing equations are modified and whose role is to absorb the incident waves, has been proposed. In this buffer zone the modifications have the effect of either removing or damping reflected waves oriented back toward the computational domain. Naturally, the buffer-zone solutions themselves need not necessarily be physical, and they serve only to prevent contamination of the solution in the physical domain of interest by the reflections from the computational boundaries. Various types of buffer-zone techniques have been used in flow simulations. For example, Colonius et al.[2] used buffer zones in which the solutions were filtered. In a different approach Ta'asan and Nark[3] modified the governing equations in the buffer zone to change the orientation of the characteristics and make the flow supersonic at the exit plane. Recently, Berenger[4] proposed a very effective perfectly matched layer technique for Maxwell's equations. In this approach the equations governing the so-called matched layer are split into subcomponents with damping terms that absorb the incident waves almost perfectly. Following Berenger, Hu[5] developed an analogous technique for the linearized Euler equations and provided analytical results for the case of uniform flow.

In this paper we follow the operator splitting principle of Berenger[4] and Hu[5] for the equations governing what we call the absorbing layers and examine their effectiveness in the case of shock-vorticity wave interactions, a plane free shear layer, and an axisymmetric jet. The emphasis is on the effectiveness of the computational boundaries in handling wave propagation including sound waves. The absorbing-layer technique is very effective for all three physical problems. The next section describes briefly the numerical models used in this study, followed by the section on results and conclusion.

Received 6 May 1997; presented as Paper 97-2075 at the AIAA 13th Computational Fluid Dynamics Conference, Snowmass Village, CO, 29 June–2 July 1997; revision received 11 January 1999; accepted for publication 9 February 1999.

*Research Scientist, Center for Research on Parallel Computation.
†Associate Professor, Department of Mathematics and Statistics.
‡Director, Program in Computational Science and Engineering.

II. Numerical Models

A. Shock-Wave Interactions

To verify the applicability of the absorbing boundary condition technique to shock-turbulence and shock-vortex interaction problems, we choose the numerical model of Erlebacher et al.[6] This model solves the fully nonlinear compressible Euler equations along with a time-evolution equation for the shock motion for the purpose of fitting the shock. The outflow boundary conditions that minimize wave reflection back into the domain of computation are of crucial importance for such problems as they involve long-time integrations. The present case focuses on the interaction of a single vorticity wave with a shock wave, and the results of course carry over simply to a randomly distributed wave system. The two-dimensional Euler equations are written as

$$\frac{\partial \rho}{\partial t} + u\frac{\partial \rho}{\partial x} + v\frac{\partial \rho}{\partial y} = -\rho\left(\frac{\partial u}{\partial x} + \frac{\partial v}{\partial y}\right)$$

$$\frac{\partial u}{\partial t} + u\frac{\partial u}{\partial x} + v\frac{\partial u}{\partial y} = -\frac{1}{\rho}\frac{\partial p}{\partial x}$$

$$\frac{\partial v}{\partial t} + u\frac{\partial v}{\partial x} + v\frac{\partial v}{\partial y} = -\frac{1}{\rho}\frac{\partial p}{\partial y}$$

$$\frac{\partial p}{\partial t} + u\frac{\partial p}{\partial x} + v\frac{\partial p}{\partial y} = -\gamma p\left(\frac{\partial u}{\partial x} + \frac{\partial v}{\partial y}\right)$$

The computational domain has the shock as a boundary on the left, an outflow boundary on the right, and is periodic in the other direction. Fourth-order Runge–Kutta scheme is used for time integration, and the spatial derivatives are discretized by a compact sixth-order scheme.

In the absorbing layer at the right boundary, the Euler equations are split into a locally one-dimensional set with artificial damping terms. Consider the pressure equation, for example, in computational space:

$$\frac{\partial p}{\partial t} = -a_1\frac{\partial p}{\partial X} - a_2\frac{\partial p}{\partial Y} - \gamma p\left(\frac{\partial w_1}{\partial X} + \frac{\partial w_2}{\partial Y}\right)$$

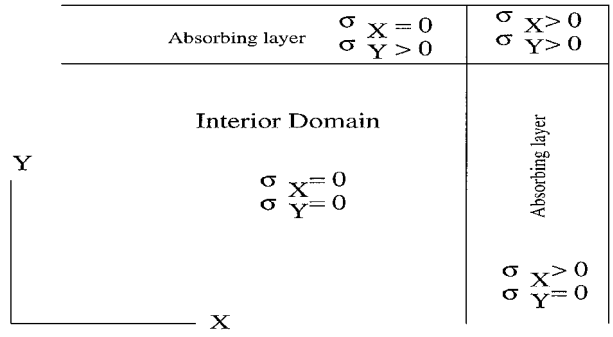

Fig. 1 Schematics of absorbing layers.

After operator splitting and addition of damping terms, the pressure equation becomes

$$\frac{\partial p_1}{\partial t} = -a_1 \frac{\partial p}{\partial X} - \gamma p \frac{\partial w_1}{\partial X} - \sigma_X p_1$$

$$\frac{\partial p_2}{\partial t} = -a_2 \frac{\partial p}{\partial Y} - \gamma p \frac{\partial w_2}{\partial Y} - \sigma_Y p_2$$

in the absorbing layer. Here, w_1 and w_2 are velocity components in the x and y directions, a_1 and a_2 are contravariant velocity components (which include the effect of grid motion) in computational space, and $p = p_1 + p_2$. Initially both p_1 and p_2 are set equal to zero in the absorbing layer. Numerical filtering is applied to the variables in the interior as well as in the absorbing layer. Locally one-dimensional equations for the other variables are constructed in a similar manner. The damping factor σ_X is zero in a layer parallel to the X direction; similarly σ_Y is zero in a layer parallel to the Y direction (Fig. 1). However, in the corner region both these damping factors are positive.

B. Free Shear Layer

To evaluate the performance of the absorbing-layer technique in the case of inviscid instability waves, we solve the linearized Euler equations in a Cartesian (x, y) coordinate system. We study the evolution of a Kelvin–Helmholtz instability wave as it propagates downstream and impinges on the absorbing layers. In this case the x-momentum equation reads

$$\frac{\partial u}{\partial t} + \bar{U}\frac{\partial u}{\partial x} + \frac{\mathrm{d}\bar{U}}{\mathrm{d}y} v + \frac{1}{\bar{\rho}}\frac{\partial p}{\partial x} = 0$$

where $\bar{U} = \frac{1}{2}[(U_1 + U_2) + (U_1 - U_2)\tanh(y)]$. Absorbing layers are used at the upper, lower, and right boundaries. Again, the aforementioned operator splitting in the absorbing layer leads to two x-momentum equations:

$$\frac{\partial u_1}{\partial t} + \sigma_x u_1 + \bar{U}\frac{\partial u}{\partial x} + \frac{1}{\bar{\rho}}\frac{\partial p}{\partial x} = 0$$

$$\frac{\partial u_2}{\partial t} + \sigma_y u_2 + \frac{\mathrm{d}\bar{U}}{\mathrm{d}y} v = 0$$

where $u = u_1 + u_2$. All other equations are treated similarly. These equations are solved by a low-dissipation and low-dispersion Runge–Kutta scheme, which is formally fourth-order accurate.[7]

For the nonlinear case one uses again an approximate time-independent mean flow to split the Euler equations in the absorbing layer. Thus the streamwise velocity for two-dimensional flows is decomposed into three components:

$$u = \bar{U} + u_1 + u_2$$

where $\bar{U}$ is the mean velocity as in the linear case. Then the x-momentum equation is written as

$$\frac{\partial u}{\partial t} + uu_x + vu_y + \frac{1}{\rho}p_x = 0$$

This equation is then split into two equations as

$$\frac{\partial u_1}{\partial t} + \sigma_x u_1 = -\frac{1}{\rho}p_x - uu_x + \frac{1}{\bar{\rho}}P_x + \bar{U}\bar{U}_x$$

$$\frac{\partial u_2}{\partial t} + \sigma_y u_2 = -vu_y$$

All other equations in the absorbing layer are similarly derived. For both linear and nonlinear shear layer computations initially split variables inside the absorbing layer are set to zero. Numerical filtering is applied to the variables in the interior as well as in the absorbing layer. We noticed numerical instabilities without added numerical dissipation (filtering). The scheme becomes stable with added numerical dissipation. Instability in computations with the absorbing layer is an important issue and has attracted the attention of many computational scientists.[8–10]

C. Axisymmetric Jet

The compressible axisymmetric Euler equations for the jet in the weak conservation form are $Q_t + F_z + G_r = S$, where, in the linearized case,

$$Q = r\begin{bmatrix}\rho\\ m_z\\ m_r\\ E\end{bmatrix}, \qquad F = r\begin{bmatrix}m_z\\ p + 2m_zU_z - \rho U_z^2\\ m_zU_y + m_rU_z - \rho U_zU_r\\ (p+E)U_z + (m_z - \rho U_z)H\end{bmatrix}$$

$$S = \begin{bmatrix}0\\ 0\\ p\\ 0\end{bmatrix}, \qquad G = r\begin{bmatrix}m_r\\ m_zU_r + m_rU_z - \rho U_zU_r\\ p + 2m_rU_r - \rho U_r^2\\ (p+E)U_r + (m_r - \rho U_r)H\end{bmatrix}$$

$$p = (\gamma - 1)\left[E - (m_zU_r + m_rU_z) + (\rho/2)\left(U_z^2 + U_r^2\right)\right]$$

In the preceding equations p, ρ, m_z, m_r, and E denote the fluctuating components of pressure, density, axial and radial momentum, total energy, and H is the mean enthalpy. These equations have been linearized around the mean velocity (U_r, U_z) represented by an error function that fits experimental measurements. The interior equations are simply split into

$$Q_t + F_z = 0, \qquad Q_t + G_r = S$$

and they are modified in the absorbing layer as

$$Q_t^1 + F_z = -\sigma_z Q^1 + S^1, \qquad Q_t^2 + G_r = -\sigma_r Q^2 + S^2$$

where $Q = Q^1 + Q^2$ and $S = S^1 + S^2$. (We used $S^1 = 0$ in this study.)

In the nonlinear case the vectors Q, S, F, and G are defined as follows:

$$Q = r\begin{bmatrix}\rho\\ \rho u\\ \rho v\\ E\end{bmatrix}, \qquad S = \begin{bmatrix}0\\ 0\\ p\\ 0\end{bmatrix}, \qquad F = r\begin{bmatrix}\rho u\\ \rho u^2 + p\\ \rho uv\\ \rho uH\end{bmatrix}$$

$$G = r\begin{bmatrix}\rho v\\ \rho uv\\ \rho v^2 + p\\ \rho vH\end{bmatrix}$$

We use the fourth-order MacCormack method, which has been successfully used in earlier studies by Hayder et al.[11] to solve the linearized Euler equations, and by Hayder et al.[12] and Mankbadi et al.[13] to solve the Navier–Stokes equations. The equations are linearized before splitting to obtain the equations for the absorbing layer. Thus, we get

$$\left(Q^1 - Q_0^1\right)_t + (F - F_0)_z = -\sigma_z\left(Q^1 - Q_0^1\right)$$

$$\left(Q^2 - Q_0^2\right)_t + (G - G_0)_r = -\sigma_r\left(Q^2 - Q_0^2\right) + (S - S_0)$$

where the subscript 0 denotes mean quantities. For the solution of the axisymmetric jet problem, split variables inside the absorbing layer are initially set to zero. No additional dissipation or filtering was added in these computations.

III. Results

In the case of the shock-vorticity wave interaction, we consider specifically the simple wave

$$u - U_1 = \epsilon U_1 2\sqrt{2}(k_y/k)\cos(k_x x + k_y y - U_1 t)$$

$$v = -\epsilon U_1 2\sqrt{2}(k_y/k)\cos(k_x x + k_y y - U_1 t)$$

$$\rho = p = T = 1$$

as the upstream condition ahead of the shock. U_1 is the upstream mean velocity normal to the undisturbed shock, $k_y = k\sin\theta$, $k_x = k\cos\theta$ (where k is upstream wave number), and $\epsilon = 0.001$ measures the intensity of the wave. Our standard interior domain is 7.4 units long with 185 uniformly spaced grid points. We used 16 points on the coordinate axis parallel to the shock. An absorbing layer abuts the right outflow boundary. We introduce damping gradually in order to minimize any reflections because of the discretization in the absorbing layer. Unless otherwise mentioned, we use $\theta =$ 30 deg, $K = 2$, and 25 grid points (=1 unit in length) in the absorbing layer for our computations. A snapshot of pressure in the interior domain at $t = 20$ is presented in Fig. 2, which shows how well the outgoing waves are absorbed with little reflection. To measure the contamination caused by reflection, the solutions are compared with a reference solution obtained by computing the flow in a much larger domain with the same spatial and temporal resolution. We follow this methodology for all problems in this study. Figure 3 compares axial variation in pressure for two different size buffers against the large domain solution at $t = 20$. Because of modifications to the governing equations, the solution in the buffer layer is irrelevant. The solution in the interior domain for a buffer with 25 points is visually indistinguishable from the larger domain solution. It has been our experience that the absorbing layer performed well in our test cases and gave results superior to traditional buffer-zone techniques.[3] We provide only limited comparisons in this paper. In Fig. 4 we compare percentage error in pressure (normalized by the amplitude of excitation and mean pressure) along the midheight of the computational domain at $t = 15$. Performance of a 10-point absorbing layer is comparable to a 100-point buffer zone. In Fig. 5 we show the rms error E in pressure at the ordinate four grid points upstream of the interface between the computational domain and the absorbing layer as a function of the layer thickness measured in the number of equidistant points. The error E is defined as

$$E = \frac{100}{|p^r_{\max}|}\sqrt{\frac{\sum_{j=1}^{N}(p^r - p)^2}{N}}$$

where p^r is the pressure from the reference solution, $|p^r_{\max}|$ is its maximum amplitude, and N is the number of grid points in the y direction ($N = 16$ in the current context). E measures the numerical error in the solution, which includes both direct and induced errors because of the interaction of residual reflections from the outflow boundary with the flow and the shock. As expected, E decreases as the layer width is increased. In Figs. 6 and 7 we show the dependence of numerical errors on the angle of incidence θ and the wave number k. The buffer layer is more effective at lower incidence angle and wave numbers, although we notice some crossovers in our numerical experiments. At later times a fraction of the reflections from the outflow boundary propagates upstream. These waves can then reflect back and forth and cause what we call induced errors. These sometimes constitute a significant portion of the errors shown in

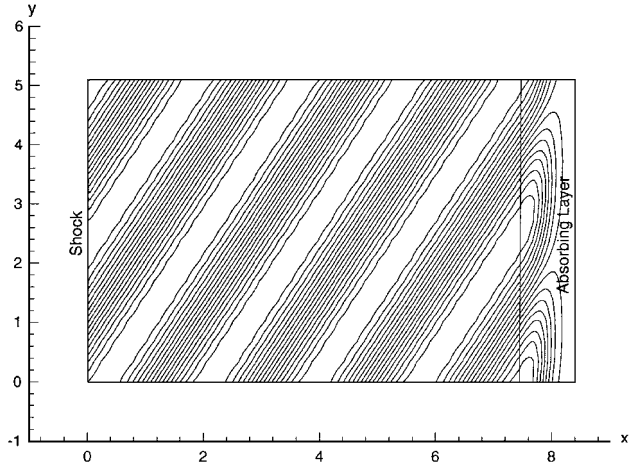

Fig. 2 Snapshot of pressure.

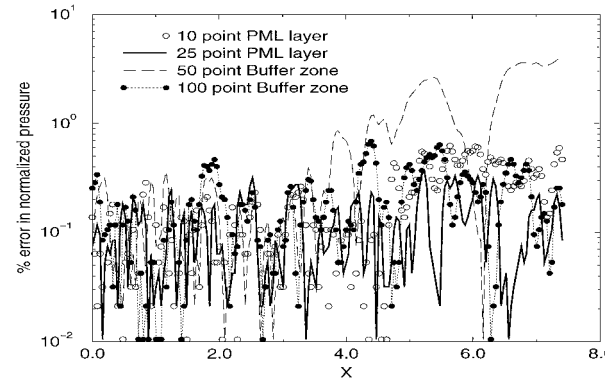

Fig. 4 Error in normalized pressure.

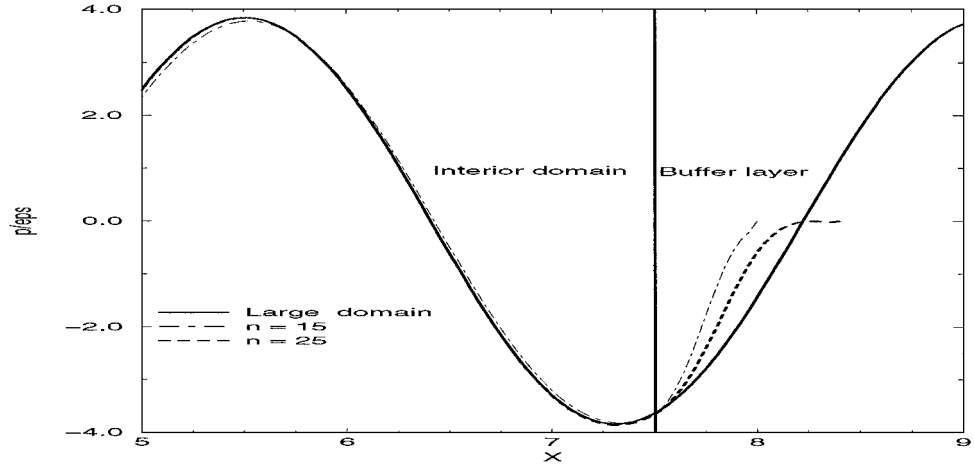

Fig. 3 Effect of buffer layer.

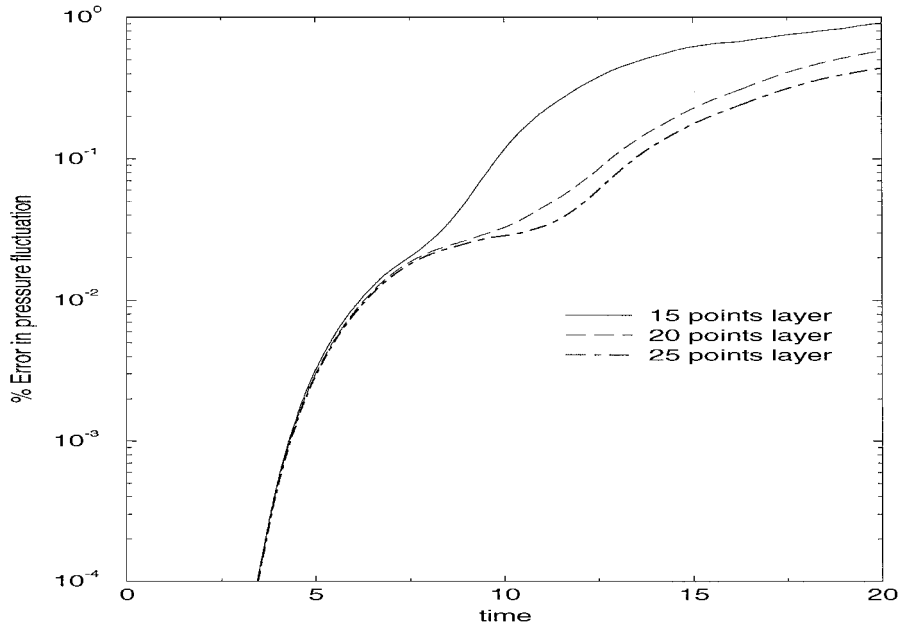

Fig. 5 Effect of layer thickness.

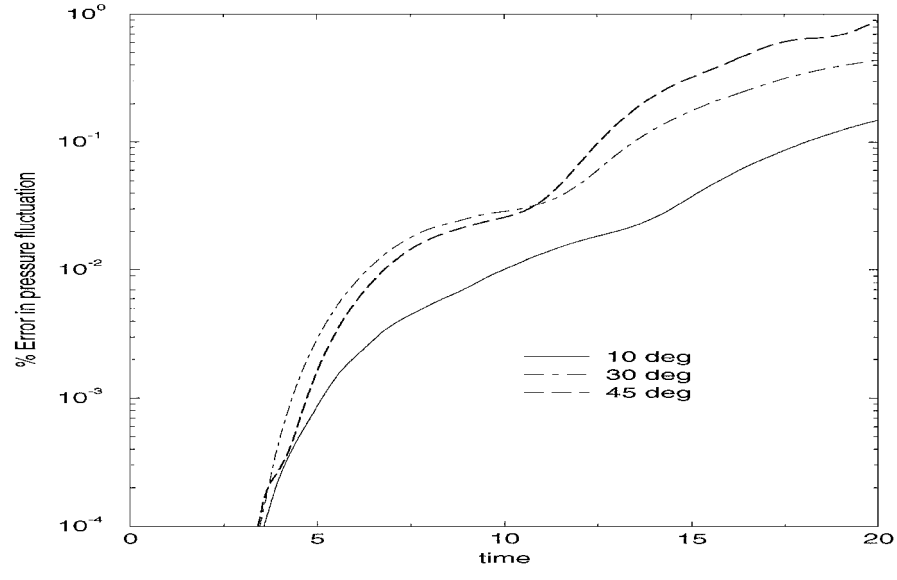

Fig. 6 Angle dependence.

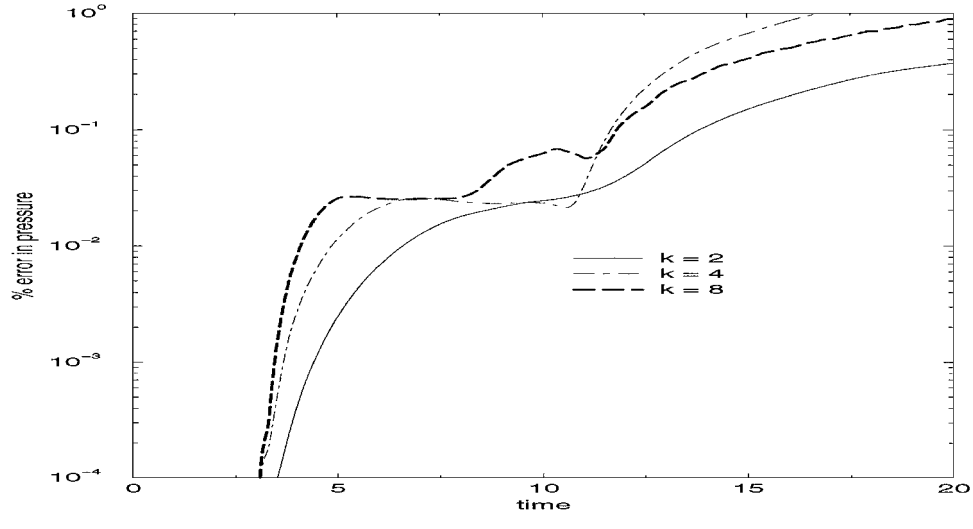

Fig. 7 Wave-number dependence.

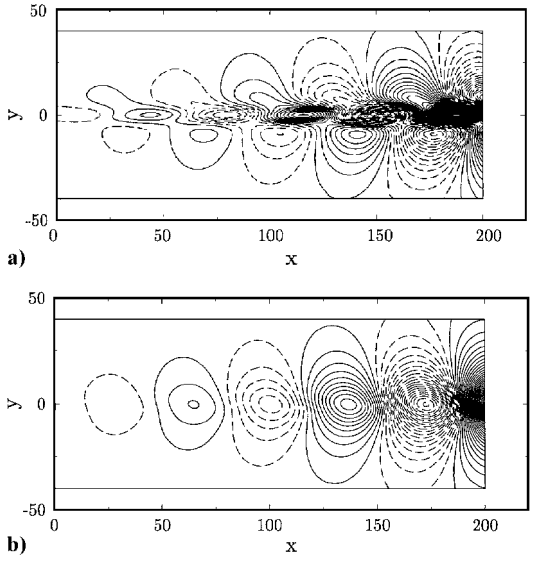

Fig. 8 Velocity and pressure contours in a free shear layer.

Figs. 5–7 at later times. As noted earlier, we used filtering in the shock-wave interaction computations and did not notice any numerical instability in the contour plots. The obvious source of long-term error growth appears to be the reflection at the boundary.

The results for the free-shear layer are obtained for upper- and lower-stream mean velocities, normalized by the speed of sound, equal to $U_1 = 0.6$ and $U_2 = 0.2$, respectively. The eigenfunctions of the Kelvin–Helmholtz instability wave given by the linear stability theory are forced at the inflow, with a maximum amplitude ϵ equal to 0.01. We solve the linearized Euler equations, and the solution agrees with the linear theory very well in eigenfunction and growth-rate comparisons. In Fig. 8 snapshots of axial velocity (Fig. 8a) and pressure (Fig. 8b) are shown. A comparison of the amount of reflection (error in normalized pressure) for two absorbing layers and a buffer zone are presented in Fig. 9. We observe that for 10 points in the absorbing layer, the amount of reflection (measured four grid points away from the buffer layer boundary) is less than 0.03% of the amplitude of the reference pressure fluctuation from the large domain solution, whereas for a 20-point buffer-zone the error (amount of reflection) is about 1.5%. We also solve nonlinear Euler equations when the nonlinearity in the flow is significant. The inflow excitation amplitude ϵ is kept

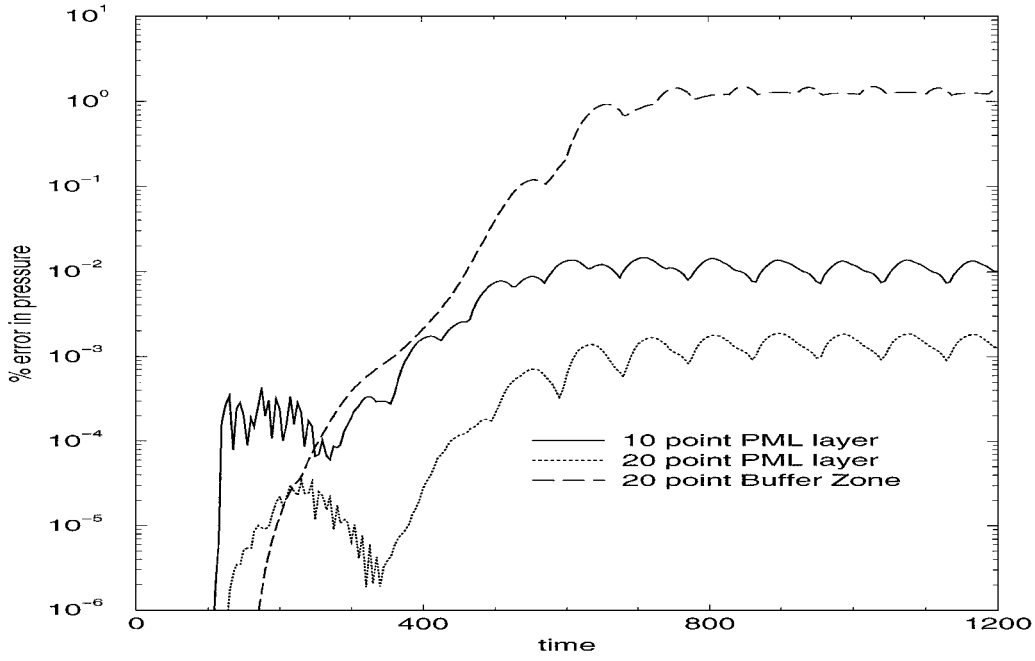

Fig. 9 Free shear layer.

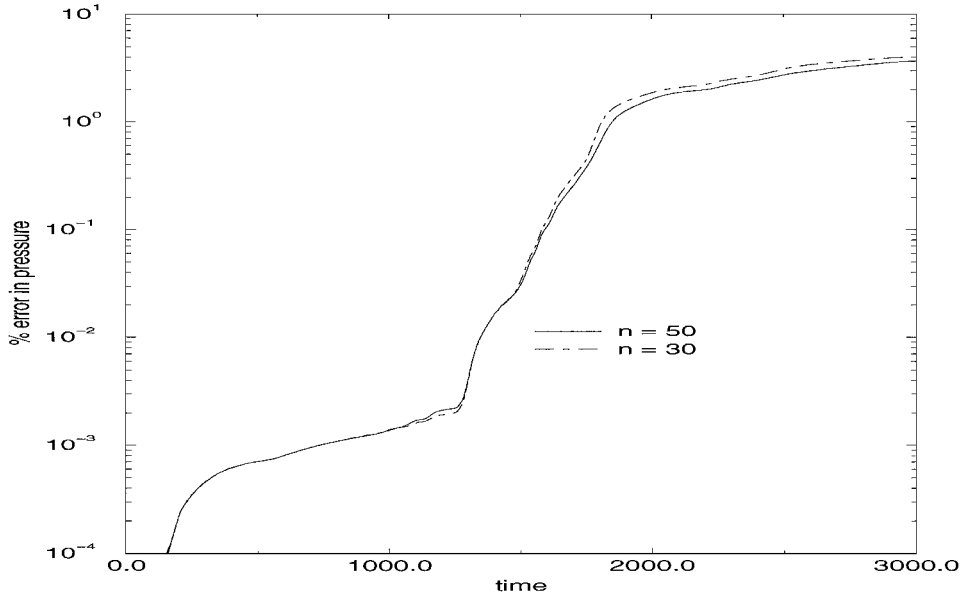

Fig. 10 Nonlinear free shear layer.

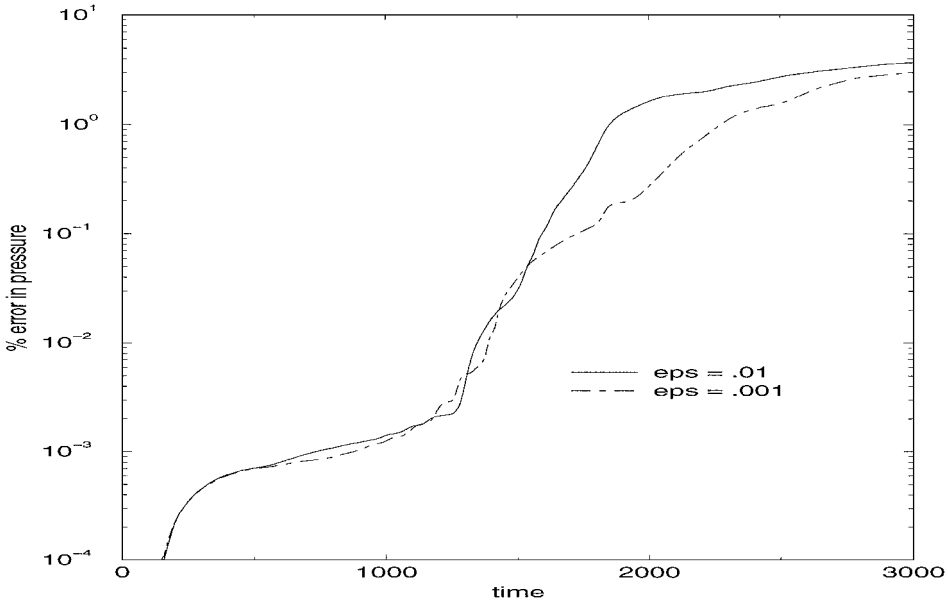

Fig. 11 Effect of excitation level.

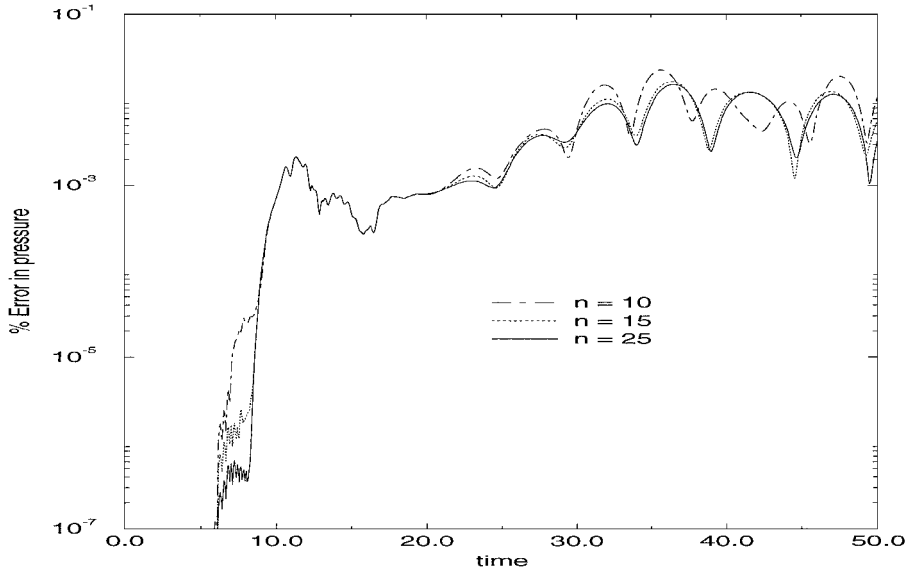

Fig. 12 Axisymmetric jet (linearized Euler).

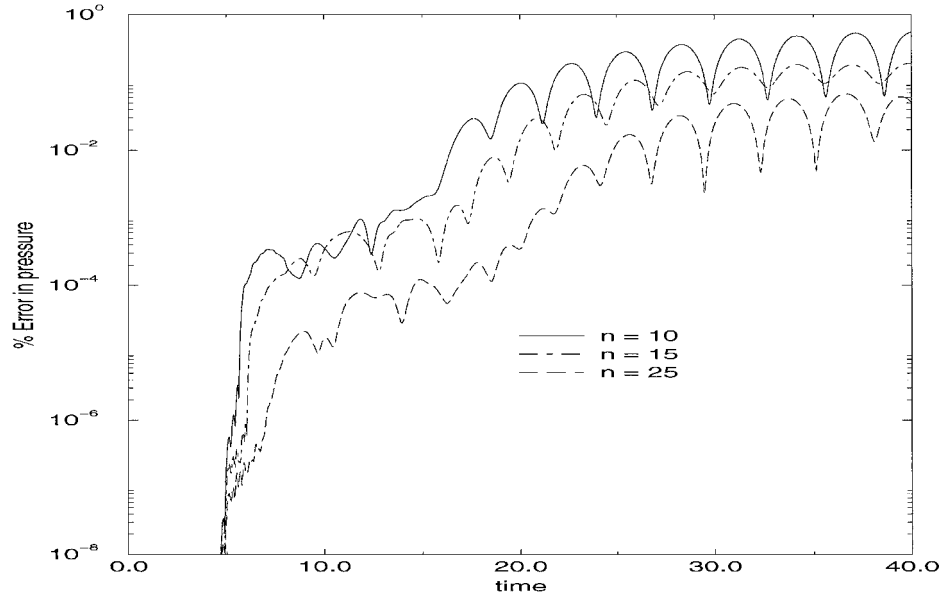

Fig. 13 Axisymmetric jet (Euler).

at 0.01, but the interior domain is three times longer. All other flow parameters are the same as in the linear case. The error in pressure four grid points away from the buffer layer is shown in Fig. 9. We needed a larger buffer layer for the nonlinear flow simulations. At time equal to 3000, errors with 30 and 50 points in the buffer layer were 3.5 and 4%, respectively. Intuitively one expects a buffer layer to be more effective if nonlinear effects are smaller. This may be the principal reason for larger errors in Fig. 10 compared to Fig. 9. The effect of nonlinearity is also shown in Fig. 11, where we compare errors for simulations with two different levels of excitation ϵ with a buffer of 50 grid points.

Finally, for the case of the excited axisymmetric jet, we assume the mean Mach number to be 0.6. At the inflow we extrapolated one characteristic variable corresponding to the outgoing acoustic wave from the interior and computed the other three characteristic variables at time t using $[\rho,\ u,\ v,\ p] = \epsilon Re(\hat{q}\, e^{i\omega t})$, where $\hat{q} = [\hat{\rho},\ \hat{u},\ \hat{v},\ \hat{p}]$ is the eigenfunction given by the linear stability theory, $\epsilon = 10^{-4}$, $\omega = 1.05$. The rms pressure error E in the immediate neighborhood (four points away from the buffer layer) of the layer interface is plotted in Fig. 12 for time up to 50. This error becomes quasiperiodic, and the maximum error for 25 grid points in the absorbing layer is about 0.015%. Our results for the nonlinear Euler equations are shown in Fig. 13. The domain size is 10 radii long for both linearized and nonlinear Euler simulations of the excited jet. The physical parameters are the same for both the linearized and the nonlinear Euler equations for the jet calculations.

IV. Conclusions

In conclusion, we find that the performance of the absorbing-layer technique in the cases of three physical problems (using three different numerical algorithms) is quite satisfactory. This technique offers a viable alternative to the traditional boundary treatments based on the linearized characteristics or asymptotic solutions in the far field and also other types of buffer layers. It also promises to be accurate and inexpensive for aeroacoustic computations. Further studies are warranted to put this methodology on a firm footing.

Acknowledgment

This research was supported by NASA under Contract NAS1-19480 while the first author was in residence at the Institute for Computer Applications in Science and Engineering, NASA Langley Research Center, Hampton, Virginia.

References

[1] Givoli, D., "Non-Reflecting Boundary Conditions," *Journal of Computational Physics*, Vol. 94, No. 1, 1991, pp. 1–29.

[2] Colonius, T., Lele, S. K., and Moin, P., "Boundary Conditions for Direct Computation of Aerodynamic Sound Generation," *AIAA Journal*, Vol. 31, No. 9, 1993, pp. 1574–1582.

[3] Ta'asan, S., and Nark, D. M., "An Absorbing Buffer Zone Technique for Acoustic Wave Propagation," AIAA Paper 95-0164, Jan. 1995.

[4] Berenger, J.-P., "A Perfectly Matched Layer for the Absorption of Electro-Magnetic Waves," *Journal of Computational Physics*, Vol. 114, No. 2, 1994, pp. 185–200.

[5] Hu, F. Q., "On Absorbing Boundary Conditions for Linearized Euler Equations by a Perfectly Matched Layer," *Journal of Computational Physics*, Vol. 129, No. 1, 1996, pp. 201–219.

[6] Erlebacher, G., Hussaini, M. Y., and Shu, C., "Interaction of a Shock with a Longitudinal Vortex," *Journal of Fluid Mechanics*, Vol. 337, April 1997, pp. 129–153.

[7] Hu, F. Q., Hussaini, M. Y., and Manthey, J. L., "Low-Dissipation and Low-Dispersion Runge–Kutta Schemes for Computational Acoustics," *Journal of Computational Physics*, Vol. 124, No. 1, 1996, pp. 177–191.

[8] Abarbanel, S., and Gottlieb, D., "A Mathematical Analysis of PML Method," *Journal of Computational Physics*, Vol. 134, No. 2, 1997, pp. 357–363.

[9] Tam, C. K. W., Auriault, L., and Cambuli, E., "Perfectly Matched Layers as an Absorbing Boundary Condition for the Linearized Euler Equations in Open and Duct Domains," *Journal of Computational Physics*, Vol. 144, No. 1, 1998, pp. 213–234.

[10] Hesthaven, J. S., "On the Analysis and Construction of Perfectly Matched Layers for the Linearized Euler Equations," *Journal of Computational Physics*, Vol. 142, No. 1, 1998, pp. 129–147.

[11] Hayder, M. E., Zhou, Y., and Rubinstein, R., "Numerical Simulation of the Mixing Noise in Turbulent Flows," *Proceedings of the Fluid Engineering Division Summer Meeting*, FED-Vol. 238, American Society of Mechanical Engineers, New York, 1996, pp. 479–484.

[12] Hayder, M. E., Turkel, E., and Mankbadi, R. R., "Numerical Simulations of a High Mach Number Jet Flow," AIAA Paper 93-0653; also NASA TM-105985, Jan. 1993.

[13] Mankbadi, R. R., Hayder, M. E., and Povinelli, L. A., "The Structure of Supersonic Jet Flow and Its Radiated Sound," *AIAA Journal*, Vol. 32, No. 5, 1994, pp. 897–906.

D. S. McRae
Associate Editor